https://doi.org/10.26565/2410-7360-2023-58-08
UDC 528.8+551.4

Received 12 April 2023
Accepted 13 May 2023

Integrating remote sensing and aeromagnetic data for lithological and structural lineaments mapping in Abu Ghaylan - Kiklah - Tighrinna, northwest Libya

Nureddin Saadi [1]
PhD (Geological Engineering), Lecturer, Department of Geological Engineering,
[1] University of Tripoli, University Road, Tripoli, Libya,
e-mail: n.saadi@uot.edu.ly, https://orcid.org/0000-0003-0593-8578;
Ousama Elkoul [2]
MSc (Geology), Lecturer, Department of Petroleum Engineering,
[2] College of Engineering Technology, Coastal Road, Janzour, Libya,
e-mail: algoul2000@gmail.com, https://orcid.org/0009-0007-3921-3045;
Saleh A. Sadeg [1]
PhD (Geological Engineering), Professor, Department of Geological Engineering,
e-mail: s.sadeg@uot.edu.ly, https://orcid.org/0000-0002-3716-3474

ABSTRACT

Problems Statement and Purpose. Libya is the fourth-largest country in Africa and the seventeenth-largest country in the world with area of 1,759,540 sq. km. Most of Libya is located in the Sahara Desert and known for being the driest and most remote regions with limited accessibility. In the 1970s, the Industrial Research Center in Libya began to create geological maps of all Libyan lands derived from analog (hard-copy) aerial photographs and geological field trips to some accessible places. Recently, remote sensing and data integration techniques using GIS are crucial to geological survey and mapping, which provides a useful tool for studying and investigating the geology of remote regions without having to physically access them. The purpose of this study is mapping lithological unites and structural lineaments in the region of Abu Ghaylan - Kiklah - Tighrinna, northwest Libya, using integrated remote sensing data and spatial analysis.

Data and Methods. Enhanced Thematic Mapper Plus (ETM+), Satellite Pour l'Observation de la Terre (SPOT 5), European Remote-Sensing Satellite-2 (ERS-2) Synthetic Aperture Radar (SAR) C-band, Digital Elevation Model (DEM), geologic maps, and aeromagnetic data were used to map and analyze the lithological and structural lineaments in the study area. Various fused images and IHS transformations were tested for lithological units recognizing. On the basis of spectral characteristics and topographic forms, lithological and structural lineaments were recognized and mapped. The extracted rasters and vectors data were integrated using remote sensing and GIS data integration techniques.

Ground Truthing. The purpose of the ground truthing was to validate the DEM-based structural mapping and identify any landslides, streams, or valleys that may appear as edges in the DEM data. Also, determining the locations of the artificial lines, that appears in the processed images as geological lineaments and edges.

Results and Discussion. The results indicate that remote sensing data were very useful in distinguishing between various rock units and recognizing geological lineaments in the study area. The generated lithologic map shows fifteen geological formations with apparent and accurate boundaries. The results exposed new geological lineaments in the study area. The direction of the extracted geological lineaments is dominantly NW-SE. The magnetic data reveal the boundary of sedimentary basin in the study area. The basement's depth within the basin varies from 122 meters to 4.5 kilometers. The extracted geological lineaments were analyzed and interpreted to provide more information about the main structural trends affecting the study area. The methods used in this study for remote sensing image analysis and field geological surveys can be used successfully in similar regions of Libya.

Keywords: *Libya, Remote Sensing, Digital Elevation, Lineaments, Lithological Mapping, Aeromagnetic, Data Integration.*

In cites: Saadi Nureddin, Elkoul Ousama, Sadeg Saleh A. (2023). Integrating remote sensing and aeromagnetic data for lithological and structural lineaments mapping in Abu Ghaylan – Kiklah – Tighrinna, Northwest Libya. Visnyk of V. N. Karazin Kharkiv National University, series "Geology. Geography. Ecology", (58), 97-110. https://doi.org/10.26565/2410-7360-2023-58-08

1. Introduction

Integration approach of multi-source data can improve geological interpretation and provide detailed information on unexplored areas [1–3]. The remote sensing satellites (sensors) can detect and map geological surface based on the spectral and spatial resolution [4, 5]. The integration method has been used to combine high spatial resolution panchromatic data with poor spatial resolution multi-spectral data. The Abu Ghaylan – Kiklah – Tighrinn area is characterized within several sedimentary and igneous rocks occurrences because of varying events during its complex geological history. Numerous old and recent geological studies were conducted on the study area, e.g. [6, 7]. This area is ideal for geological remote sensing study because of its inaccessibility and lack of vegetation. This study emphasizes the importance of fusing and integrating multi-source remote sensing and aeromagnetic data for geological mapping [8–10]. Optical-radar- Digital Elevation Model (DEM) remote sensing data integration was used in this study for: (1) Distinguishing the spatial distribution of

basalt flows, basalt cones and phonolite intrusions by integrating Landsat Enhanced Thematic Mapper Plus (ETM+) thermal infrared (TIR) data with band-ratio of SPOT 5 visible and near infrared (VNIR) and Synthetic Aperture Radar (ERS-2 SAR) C-band. (2) Fusion of ETM+, SPOT 5 and ERS-2 images has been tested to accurately identify further lithological units. (3) Extracting and mapping geological lineaments using DEM data. The DEM were used to extract and map geological lineaments and obscure artificial lineaments in the study area.

Furthermore, DEM were also used to avoid bias caused by the illumination direction. Shaded relief maps and slope maps were created and analyzed using DEM derivatives. Ground truthing was done for confirming the remote sensing implications and determining the artificial lines, which could eventually generate edges on the remote sensing data.

The geophysical data used to delineate the subsurface structural features and estimate the depth of the basement [11, 12]. We used aeromagnetic data to gain a broad overview of the subsurface structure in the study area. Horizontal Gradient (HG) filter was used to locate the edges of the subsurface structures [13, 14]. According to a qualitative analysis of the aeromagnetic data, the study area is distinguished by a sizable, northwest-trending positive magnetic anomaly. The analysis of the aeromagnetic data revealed that the depth of the basement ranges from 122 m to 4.5 km.

The new results modified formation boundaries, distinguished between several rock units, and exposed new geological lineaments in the study area. The new geological map was created using modified formation boundaries; fifteen rock units were identified and plotted in the map. New information about the main structural trends of the study area was obtained by analysis and interpretation of the extracted geological lineaments and the age of the geological formations.

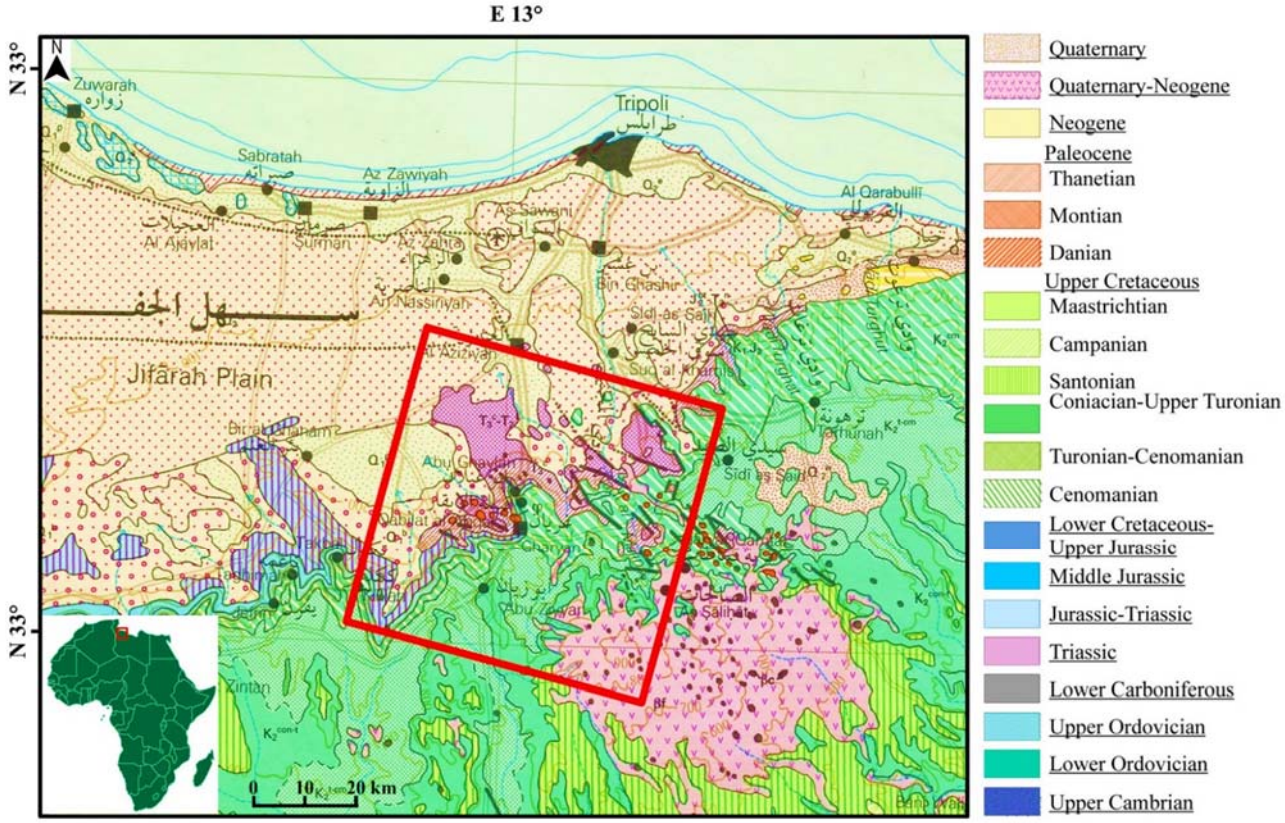

Fig. 1. Geological map of NW Libya [15]. Location of study area shown in red outline

2. Geological Setting

The study area lies in the northwestern part of Libya on the Jabal Nafusah, bounded by longitudes 12°45E to 13°20E and latitudes 32°00N to 32°27N (Fig. 1). It covers a surface area of approximately 3500 km2. The Jabal Nafusah extends roughly east-west direction from the Mediterranean Sea and westward till it reaches beyond the Libyan border. It is elevated between 500 and 700 meters above sea level and overlooks the Sahl Jifara. The Jabal Nafusah is built by Mesozoic rocks, which are made of limestone, sandstone, clay and dolomitic limestone [16]. The origin of the Scarp (Jabal Nafusah) was a subject of two different opinions. The first conclusion was mentioned by [17] who asserted that the Jabal front is an elevated sea cliff that was ravaged on the northern side by waves while the Sahl Jifara was still under water. The second conclusion was described by [18] and [16] who attributed the formation of the scarp to the Al Aziziyah Fault which took place in pre-

Miocene time. The Plateau is a Questa primarily composed of Upper Cretaceous dolomitic limestone, which is hard and resistant. Basalt sheets and black hills of phonolite and basalt are spread throughout the southeast region [19]. The basalt sheet's age was determined by [20] as early Eocene to Pliocene, whereas the basalt at Wadi Ghan was interpreted by [21] as early Quaternary. Ages of the sedimentary rocks exposed in the study area range from the Triassic to the Quaternary. Quaternary sediments are particularly observed on the northern part of the study area.

3. Remote Sensing Data and Methods

In this study, optical, radar, and DEM remote sensing datasets were used and experimented. The optical data include ETM+ and SPOT 5. The radar data was represented by Synthetic Aperture Radar (ERS-2 SAR) C band. The DEM are extracted from topographic maps (1:50,000). Fused image from ETM+ thermal infrared (TIR) band, SPOT 5 visible and near infrared (VNIR) bands and ERS-2 SAR C-band is used in this work. The spectral characteristics of the ETM+ (TIR), SPOT 5 (VNIR) and ERS-2 C band tested in this study found to be remarkably successful in geological mapping, particularly at differentiating between lava flows with various compositions. Fused images from other bands of ETM+, SPOT 5 and ERS-2 C band have been effectively implemented for further lithological units recognizing. Data from multi-spectral optical and radar sources were combined using the Intensity-Hue-Saturation (IHS)-RGB transformation. Based on the predominant wavelength, hue is used to define the color, saturation determines the purity, while intensity used to define the brightness [22]. Thus, while the radar data are used to define the intensity, the multi-spectral data of the ETM+ and SPOT 5 are used to define the hue and saturation. Data transformations and image ratios help to increase the accuracy of land classification. They can also eliminate redundant data [23].

Generating and analyzing DEM derivatives, such as shaded relief maps and slope maps, were used to identify and map landforms and structural boundaries [24]. These extracted maps were useful in examining how morphology and structures relate to one another.

3.1. Lithology

Three different types of volcanic rocks are exposed on the surface of the study area: basalt flows, basalt cones, and phonolite intrusions. The ETM+ TIR band (distinguishes different volcanic rocks) was integrated with SPOT 5 band-ratio 3/1 (NIR/G) (high spatial resolution) and ERS-2 C band (ability of penetration) for discriminating different volcanic rocks in the study area (Fig. 2). Several fused images from ETM+, SPOT 5 and ERS-2 data were generated to enhance the visual interpretation. These images included: IHS- RGB SPOT 5 (NIR), SPOT 5 (SWIR) and ERS-2 C band; IHS-RGB- ETM+ (TIR), SPOT 5 (NIR) and SPOT 5 (SWIR); HIS RGB- ETM+ (TIR), SPOT 5 (G) and ERS-2 C band; IHS- RGB-SPOT 5 (NIR/G), ETM+ (5/7) and ERS-2 C band (Fig. 3 and 4).

The electromagnetic spectrum's VNIR portion has the ability of preserving morphological features and exhibiting various lithological units in easily distinguishable colors [25]. Clay minerals have a substantial absorption property in the mid-infrared portion, making it possible to differentiate clay units using this band [25]. Iron oxides have a high reflectance in the near infrared band (NIR), which is useful for mapping iron oxides [26]. The wavelength for the color green (vegetation) is matched by the green band [25]. The moisture content of vegetation and soils, also geological and vegetation mapping were all done using the bands G-NIR-SWIR. These bands are useful for geological mapping in arid regions due to lack of vegetation cover.

3.2. Structure

DEM constructed from topographic contour maps (1:50,000) [27], which scanned, geo-referenced, and digitized. The topographic maps have contour interval of 20 m, in addition to the 10 m intervals as supplementary contours. The generated DEM has a 20 m horizontal resolution and a 5 m vertical resolution. To detect and map geological lineaments in the study area, a number of image processing techniques were applied to the digital elevation data to produce shaded relief maps and slope maps.

In the processing of shaded relief maps, the incoming illumination that is perpendicular to the predominant trend of geological lineaments in the study area was evaluating. The published geology map of the study area shows that the predominant lineaments trend in NW-SE directions [15]. In order to reduce azimuth biasing effects and improve the visual detection of geological lineaments in the dominant trend, low incoming solar radiation from the NE-NNE was experimented. To avoid azimuth-biasing effects, four azimuth angles of simulated sun light (NENNE, NW-NNW, NW-WWN, and N) were examined. For lineament detection in all directions, a low sun elevation angle (20° to 30°) was used (Fig. 5).

Using a quadratic fitted to a 3×3 kernel, a slope map was produced. There is no weighted convolution array used in the 3×3 filter, which is written in C code. This slope filter produces data values in degrees from horizontal. Slope values in the output image range from 0° (flat terrain) to 90° (vertical terrain). White areas represent the sharpest slopes and black areas represent the gentlest slopes in an 8-bit panchromatic image (Fig. 6). Topographic lineaments can be identified by their elevation difference from the adjacent topography. The colors of the slope map

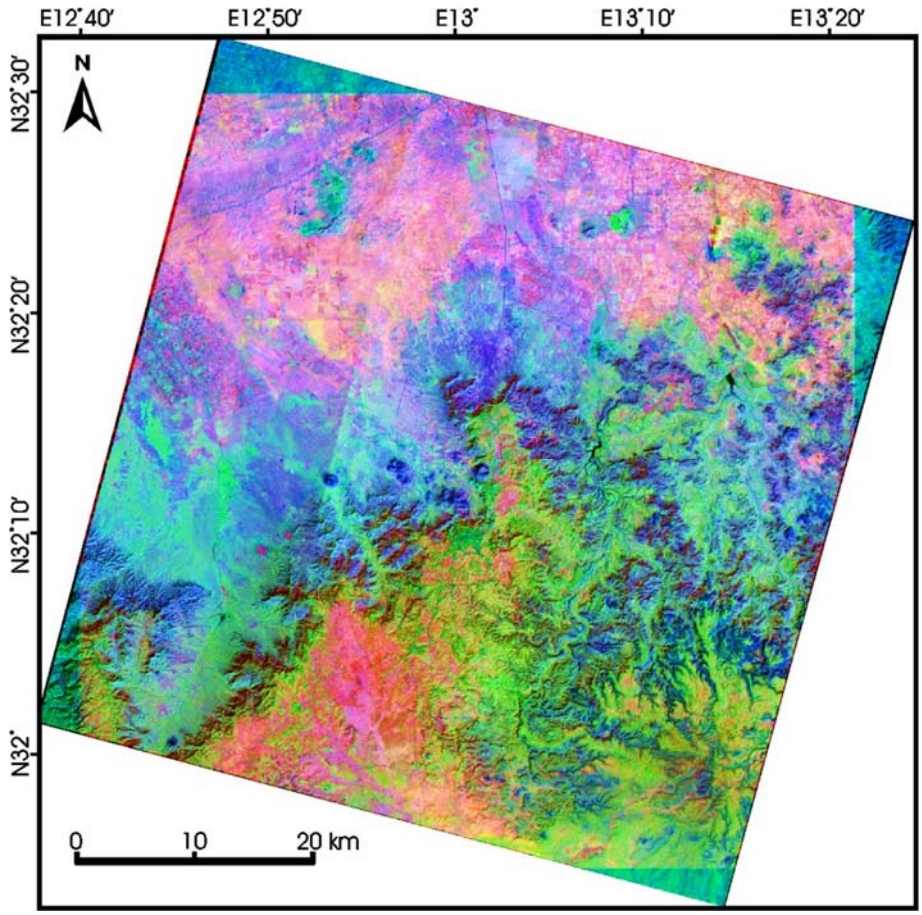

Fig. 2. ETM+ TIR band fused with ERS-2 C band and SPOT 5 NIR/G band-ratio

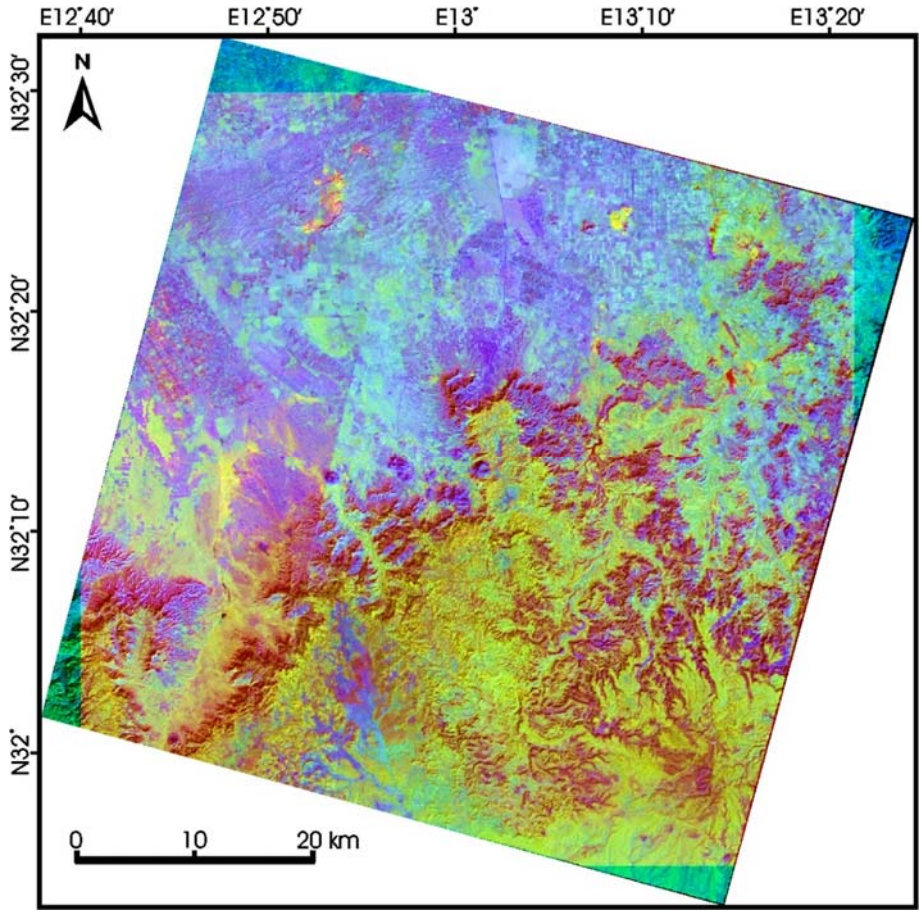

Fig. 3. ETM+ TIR band fused with ERS-2 C band and SPOT 5 G band

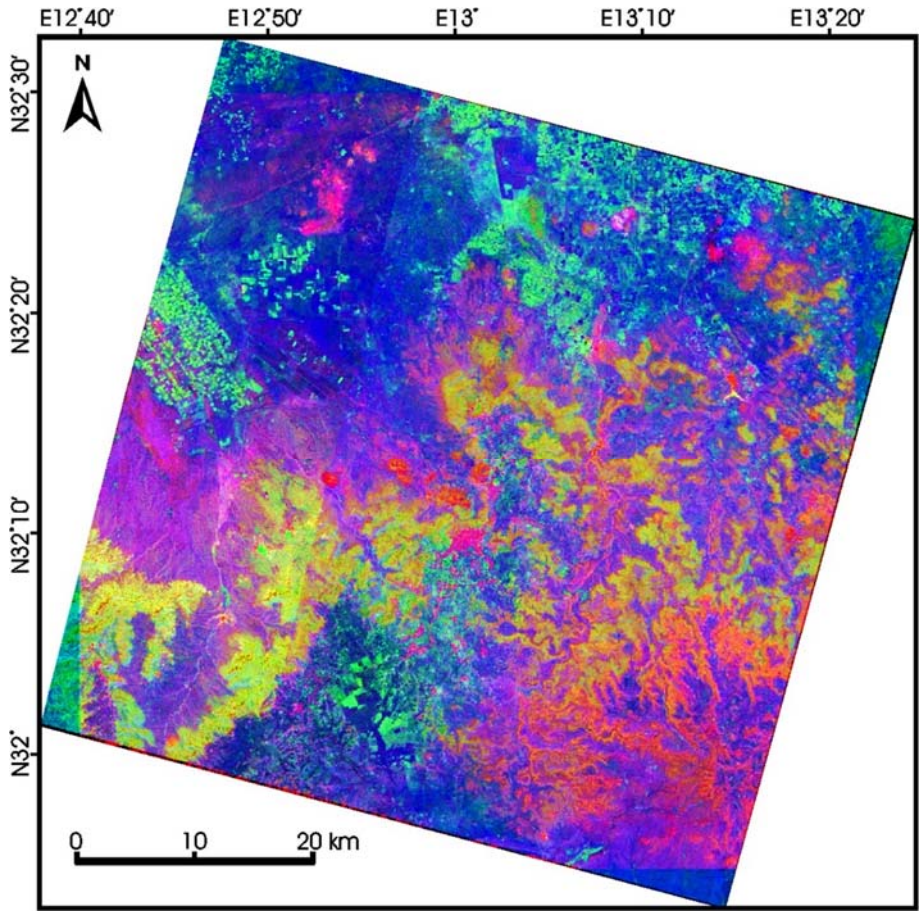

Fig. 4. ETM+ 5/7 band ratio fused with ERS-2 C band and SPOT 5 NIR/G band-ratio

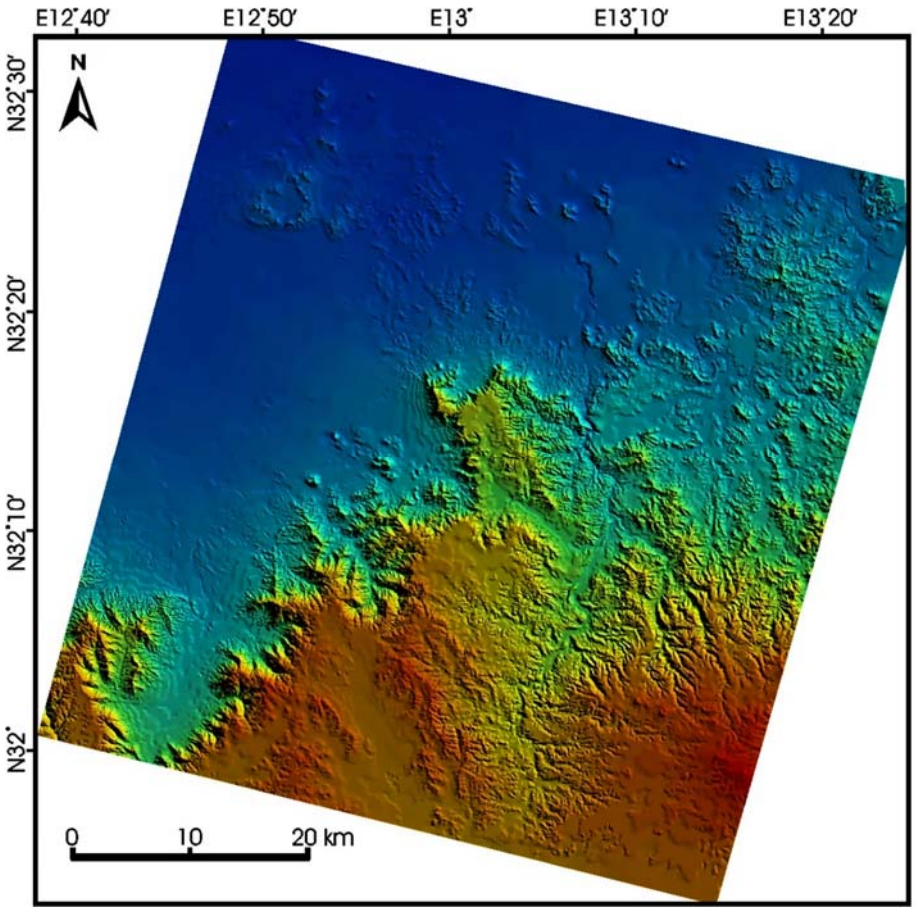

Fig. 5. The shaded relief map, azimuth angle is NE-NNE and sun-elevation is 27º

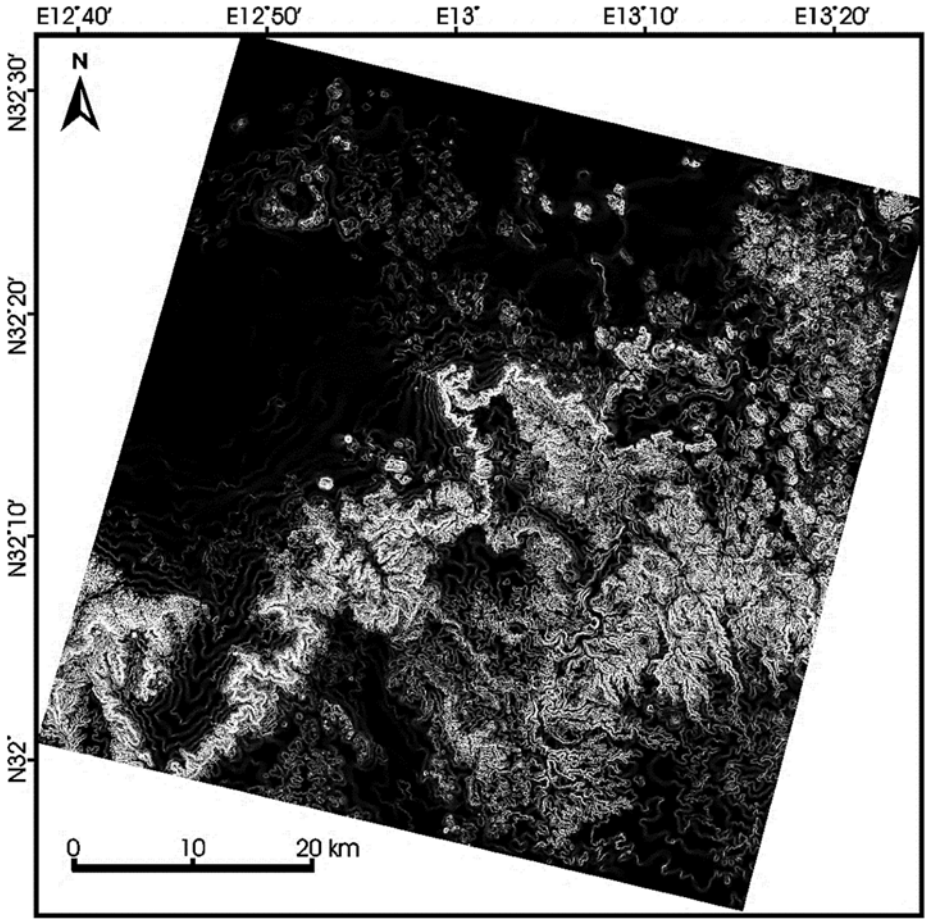

Fig. 6. The slope map. Black areas have the gentlest slopes, whereas white areas have the steepest slopes

can reflects the elevation changes in the study area.

The extracted lineaments were overlaid on a map shows the age of the geological formations in the study area (Fig. 7). The principle of cross-cutting relationships was used as the foundation for the analysis and interpretation of these lineaments [28, 29].

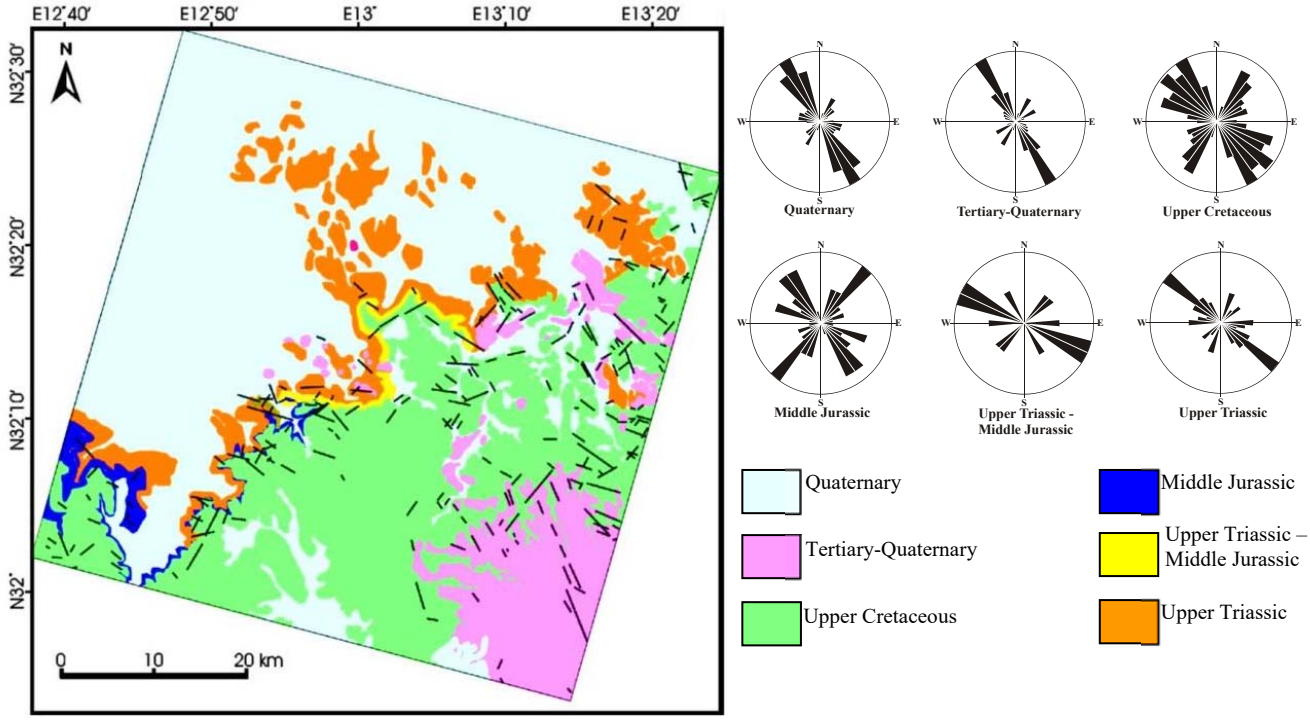

Fig. 7. Lineaments extracted from the DEM overlaid on geological formations map organized by age along with the rose diagram of each age

4. Magnetic Data Analysis

Corrections were made to the aeromagnetic survey data, including the International Geomagnetic Reference Field (IGRF). The Total Magnetic Intensity (TMI) of the investigated area is shown in Figure 8.

According to a qualitative analysis of the magnetic data (Fig. 8), the study area is characterized by a sizable positive anomaly in the central (red-pink color). This anomaly has a maximum value of ~190 nT in the middle and values of ~9 nT on the troughs, and it tends NW-SE.

The anomalies and edges that directly connect to the structure are enhanced and made more distinct by filtering the magnetic data. The structure's edges were located using the Horizontal Gradient (HG) filter [30]. The key benefit of the HG filter is that it emphasizes the maximum anomaly values at the edges (faults/borders) of the primary structure (Fig. 9). Once the maxima have been identified, other techniques can be used to determine the depths and trends of the borders from the HG map. In order to recognize the subsurface structure and more thoroughly investigate the anomaly, we applied a depth estimate approach to the HG data output. Figure 10 shows the depth maps from HG data.

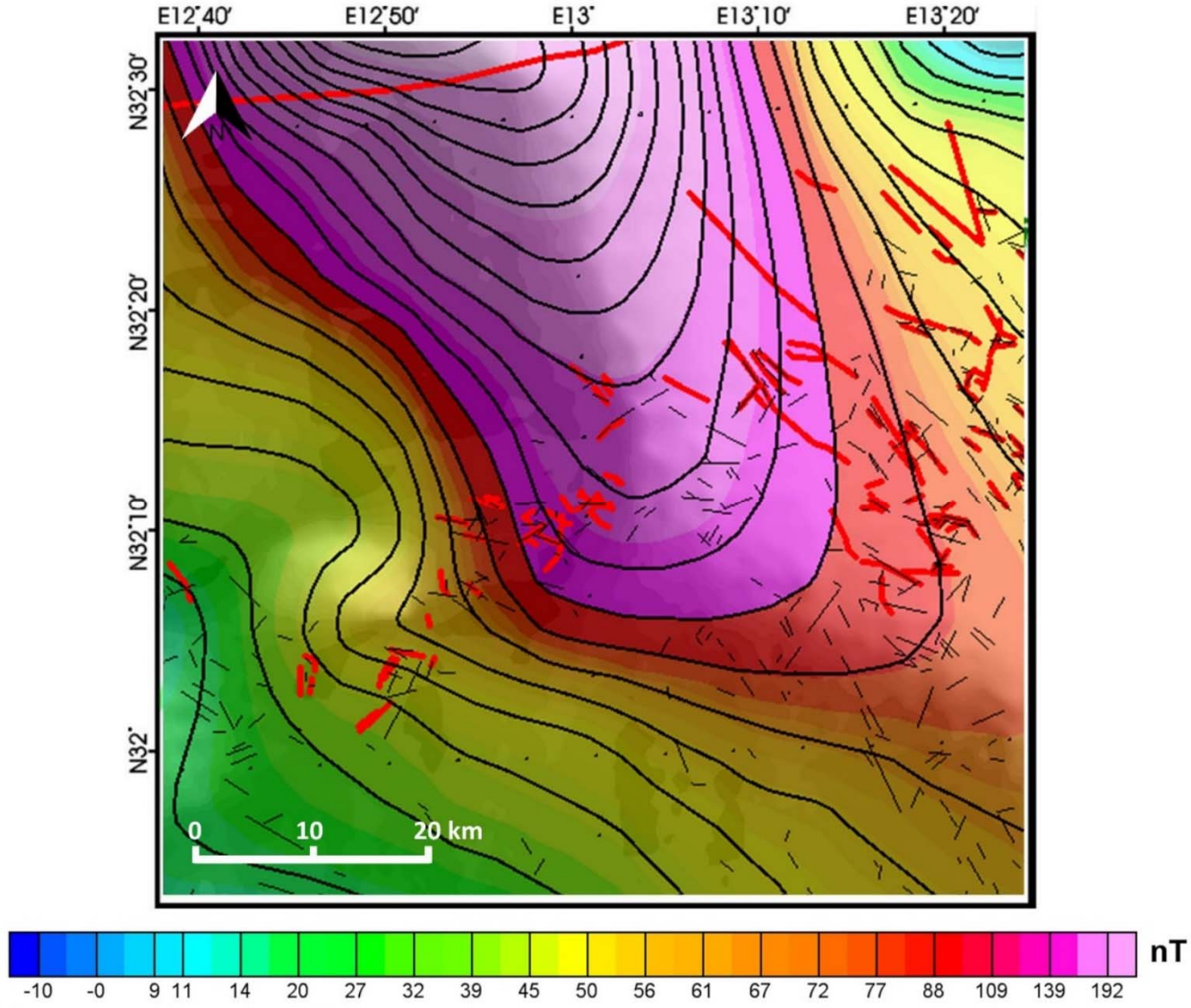

Fig. 8. Total magnetic intensity map. C.I. = 10 nT. Grid cell size equals 500 m. Geologic faults traced from the published geological map are shown as red lines [15]. The geological lineaments extracted from the DEM are shown as fine black lines

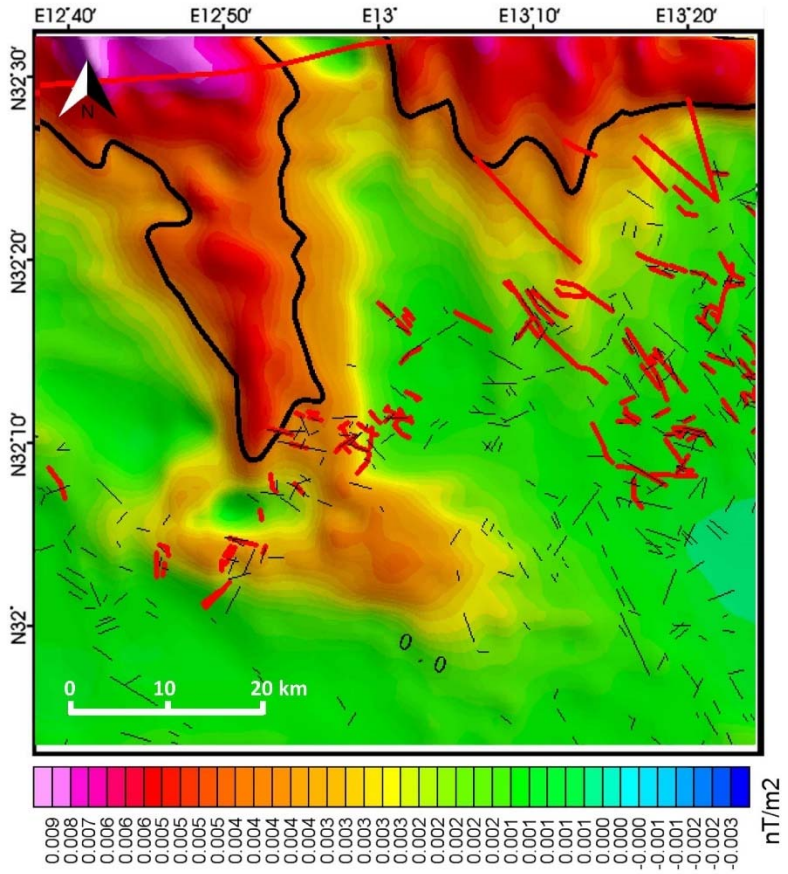

Fig. 9. Horizontal gradient map. Geologic faults traced from the published geological map are shown as red lines [15]. The geological lineaments extracted from the DEM are shown as fine black lines

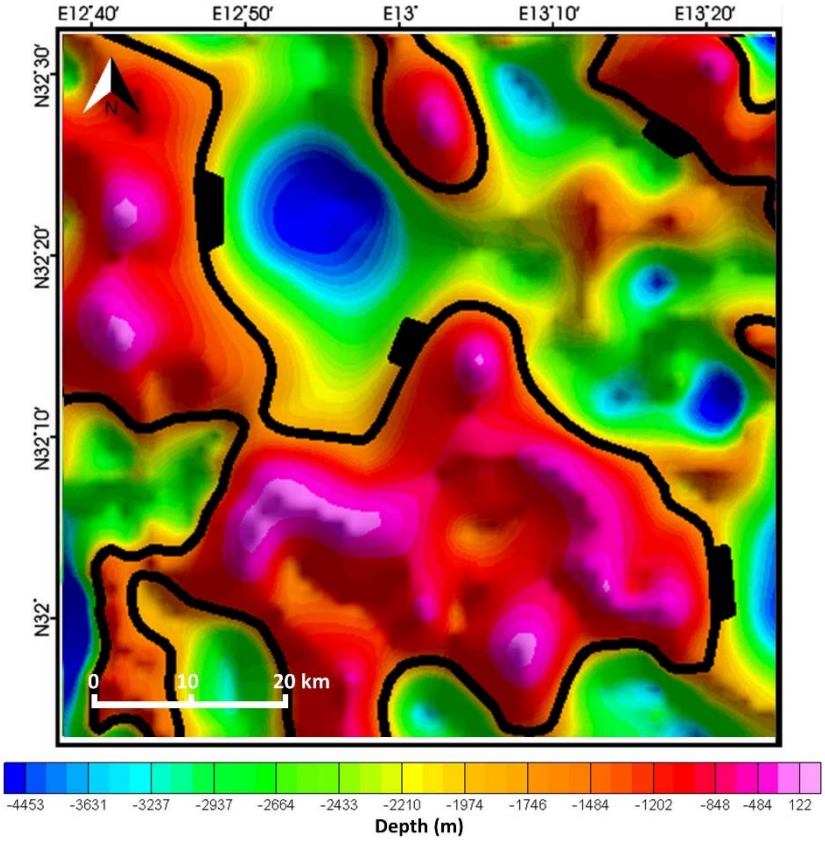

Fig. 10. Depth map from the horizontal gradient. The colors represent depth. The solid black line represents the edges of the subsurface basin

5. Ground Truthing

Ground truthing focused on: (i) confirming the DEM-based structural mapping and (ii) determining the landslides, streams and valleys that may potentially cause edges to appear on the DEM data. Ground truthing revealed that the study area is dominantly covered with Quaternary sediments. The scarp is mostly built by limestone, sandstone and clay. The soft rocks form the slopes, which are often covered by debris and limestone mass. Conspicuous black hills made of phonolite and basalt are frequently observed in the southeast region (Fig. 11, 12, 13 and 14).

Fig. 11. Normal fault in Abu Ghaylan Formation

Fig. 12. Well bedded limestone of the Ain Tobi Member (Sidi as Sid Formation)

Fig. 13. The Plateau (Dahr) in southeast of the study area

Fig. 14. A general view of the study area in which geological formations are shown

6. Results and Discussion

The results show that SPOT 5, ETM+ and ERS-2 SAR sensors are capable of differentiating between different rock units and identifying geological lineaments in the study area. The IHS-RGB- ETM+ TIR, SPOT 5 (NIR/G) and ERS-2 C fused image was able to differentiate more lithological units than other fused images. It was possible to distinguish between areas dominated by bedrock covered in thin sand and those that are covered in thick sand using the SPOT 5 and ERS-2 C fused image. On the new lithologic map, the following fifteen rock units were identified (Fig. 15). The published geological map and Ground truthing were used for confirming these results.

i. Al Aziziyah Formation: The primary material in this unit is bedded limestone, which is distinguished by its dark grey color. Al Aziziyah Formation was mainly recognized by the fused image IHS-RGB- SPOT 5 (NIR), SPOT 5 (SWIR), and ERS-2 C band.
ii. Abu Shaybah Formation: Sandstone layers alternate with layers of clays and and scattered limey bands. The fused image IHS-RGB- ETM+ (TIR), SPOT 5 (NIR/G), and ERS-2 C band was used to recognize this formation.
iii. Abu Ghaylan Formation: Mostly limestone makes up this formation. Using the fused image IHS-RGB-SPOT 5 (NIR), SPOT 5 (SWIR), and ERS-2 C band was successful in recognizing this formation.
iv. Bir al Ghanam Formation: Mainly consists of gypsum, anhydrites and dolomites. Fused image HIS-RGB-ETM+ (TIR), SPOT 5 (NIR/G), and ERS-2 C band was utilized to recognize this formation.
v. Takbal Formation: Mainly limestone with marly and clayey intercalations. Fused image IHS-RGB- ETM+ (TIR), SPOT 5 (NIR) and SPOT 5 (SWIR) was useful for identifying this formation.
vi. Sidi as Sid Formation: Mostly limestone and marl. This formation was recognized using fused image IHS-RGB- SPOT 5 (NIR/G), ETM+ (5/7) and ERS-2 C band.
vii. Nalut Formation: It consists of limestone and dolomitic limestone. Nalut Formation was recognized using fused image IHS-RGB SPOT 5 (NIR/G), ETM+ (5/7) and ERS-2 C band.
viii. Qasr Tigrinnah Formation: This unit consists of a succession of soft marls and white to rosy limestone. The fused image IHS-RGB- ETM+ (TIR), SPOT 5 (G) and ERS-2 C band was used to recognize this formation.
ix. Volcanic rocks: This formation consists of basalt flows, basalt cones, and phonolite intrusions. We used fused image IHS-RGB- SPOT 5 (NIR), SPOT 5 (SWIR) and ERS-2 C band for distinguishing volcanic rocks.
x. Quaternary: The Jifara Formation, Qasr Al Haj Formation, eolian deposits, and fluvio-eolian deposits were the only types of Quaternary sediments discriminated in the study area. These sediments were recognized using fused images IHS-RGBETM+ (TIR), SPOT 5 (NIR/G), and ERS-2 C band and IHS-RGB- SPOT 5 (NIR/G), ETM+ (5/7) and ERS-2 C band.

Structurally, 233 geological lineaments were identified using the DEM data (Fig. 7). For detecting lineaments, a low illumination angle was ideal. Different trends can be seen in the extracted lineaments, but the dominant trend is NW-SE, which is parallel to the main tectonic of the Jabal Uplift. A secondary trend is the NE-SW lineaments. The rest of the trends have no statistical significance. According to geological formations ages in the study area, the extracted lineaments were divided into six groups (Fig. 7). The dominant trend of lineaments in the Upper Triassic rocks is NW-SE, with subordinate E-W and NE-SW. Rocks from the Upper Triassic and Middle Jurassic shows lineaments trend dominantly NW-SE, with E-W and NE-SW subordinate trends. The NE-SW trend dominates the Middle Jurassic rock lineaments, with the NW-SE is the second dominant trend. The NW-SE is the prevailing trend of lineaments in Upper

Cretaceous rocks, the NE-SW trend being subordinate. Lineaments in Tertiary rocks trend dominantly NW-SE, with a subordinate trend to the NE-SW. Lineaments in Quaternary rocks prevailingly trends NW-SE.

The principle of cross-cutting relationships was used as a foundation for the analysis of the extracted lineaments [28]. Possibility of reactivated faulting in the Upper Triassic and Upper Cretaceous rocks, as indicated by the frequency and length of NW-SE faults. The varying lengths of the NW-SE lineaments in the Upper Cretaceous rocks likely imply reactivated faulting. Lithologically, the arrangement of basalt cones and phonolite hills in lines parallel to the prevailing lineaments trends (NW-SE) shows a relation between the tectonic activity of the Jabal Uplift and the volcanic activity in the study area.

The magnetic data shows an area of anomalously high values in the center of the study area, and two areas of anomalously low values in the northeast and southwest. The magnetic data reveal the edges of the subsurface basin, which trends NW-SE, and its depth varies from 122 m to 4.5 km. The abrupt change in the magnetic anomaly reveals a basement fault. Variations in trend and depth indicate that the studied region was active at several stages. Notably, basalt intrusion (underneath extrusive basalt flow in the study area) does not appear on the magnetic intensity map. This is may be because basaltic rocks are hydrothermally altered.

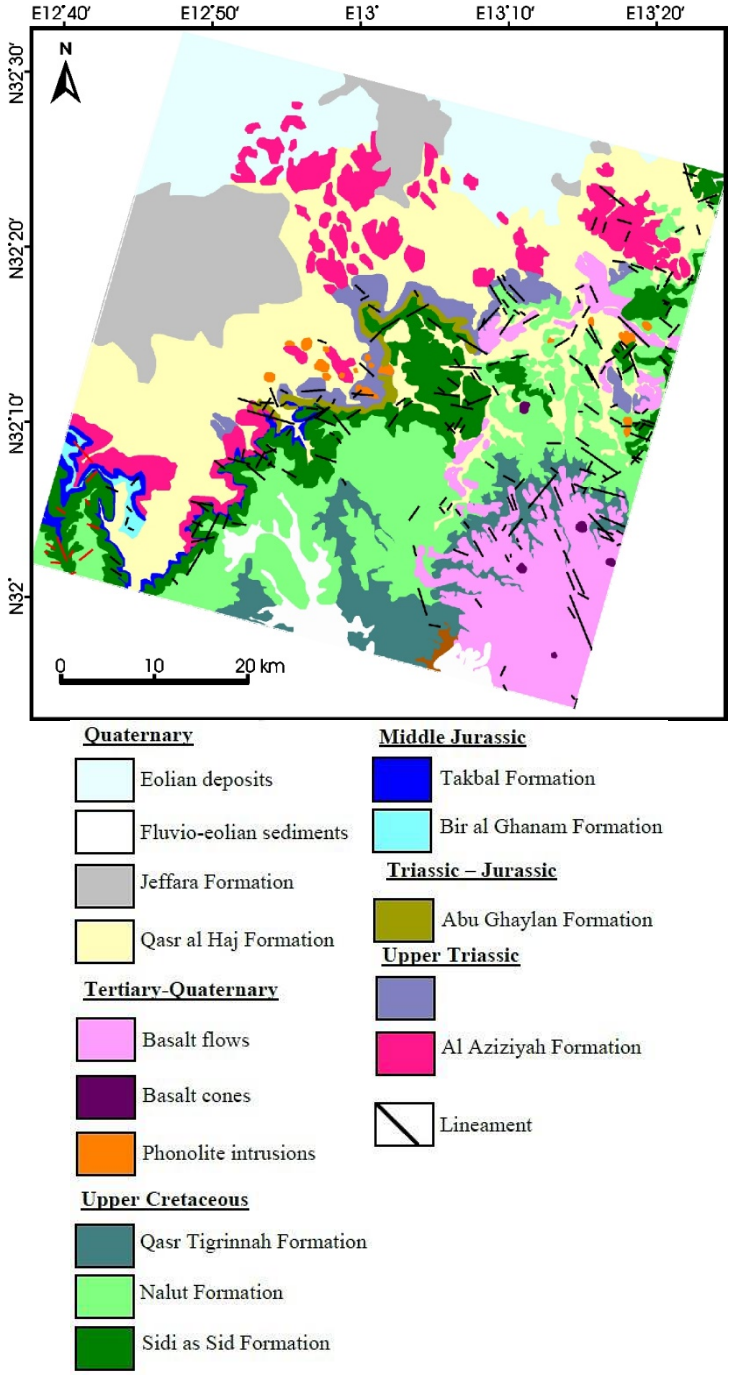

Fig. 15. New lithologic map shows the distribution of fifteen rock units and extracted lineaments in the study area

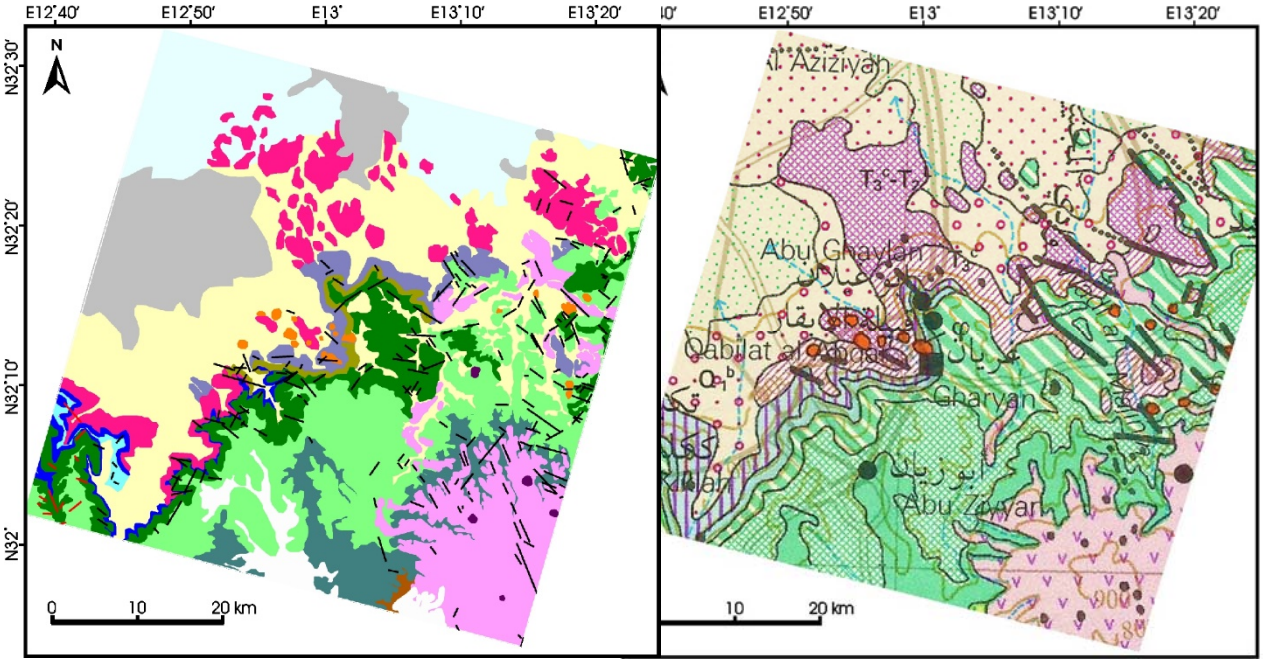

Fig. 16. Generated lithologic map (left) reveals the accurate distribution of the major geological formations of the study area with high-contrast boundaries of rock units in compare to the published geological map (right)

7. Conclusions

This study focused on geological mapping and structural analysis using various digital image processing techniques. The integration of SPOT 5, ETM+ and ERS-2 C band revealed the accurate distribution of the major geological formations of the study area with high-contrast boundaries of rock units. The DEM and aeromagnetic data provided insight into the structure of the investigated area. IHS-RGB- ETM+ (TIR), SPOT 5 (NIR/G), and ERS-2 C band and IHSRGB- SPOT 5 (NIR/G), ETM+ (5/7) and ERS-2 C band fused images successfully identified different lithological units. The shaded relief and slope maps constructed from DEM facilitated the recognition and extraction of geological lineaments. Information on the main structural trends affected the study area was obtained by classifying the extracted lineaments into groups according to the age of geological formations. Such an approach of remote sensing image analysis and field geological surveys can be successfully adopted in other arid regions in Libya.

References

1. *Thiele, S.T., Lorenz, S., Kirsch, M., Cecilia Contreras Acosta, I., Tusa, L., Herrmann, E., Möckel, R., Gloaguen, R. (2021). Multi-Scale, Multi-Sensor Data Integration for Automated 3-D Geological Mapping. Ore Geology Reviews, 136, 104252. DOI: https://doi.org/10.1016/j.oregeorev.2021.104252*
2. *Shebl, A., Abdellatif, M., Elkhateeb, S.O., Csámer, Á. (2021). Multisource data analysis for gold potentiality mapping of Atalla area and its environs, Central Eastern Desert, Egypt. Minerals, 11(6), 641. DOI: https://doi.org/10.3390/min11060641*
3. *Wróbel, M., Stan-Kłeczek, I., Marciniak, A., Majdański, M., Kowalczyk, S., Nawrot, A., Cader, J. (2022). Integrated Geophysical Imaging and Remote Sensing for Enhancing Geological Interpretation of Landslides with Uncertainty Estimation–A Case Study from Cisiec, Poland. Remote Sensing, 15(1), 238. DOI: https://doi.org/10.3390/rs15010238.*
4. *Khalifa, A., Bashir, B., Alsalman, A., Öğretmen, N. (2021). Morpho-tectonic Assessment of the Abu-Dabbab Area, Eastern Desert, Egypt: Insights from Remote Sensing and Geospatial Analysis. International Journal of Geo-Information, 10(11), 784. DOI: https://doi.org/10.3390/ijgi10110784*
5. *Lu, Y., Yang, C., Meng, Z. (2021). Lithology discrimination using sentinel-1 dual-pol data and SRTM data. Remote Sensing. 13 (7), 1280. DOI: https://doi.org/10.3390/rs13071280*
6. *Salem, M.J., Oun, K.M., Seddiq, H.M. (2003). The Geology of Northwest Libya II: Second Symposium on the Sedimentary Basin of Libya, Tripoli, Libya, 3, 123-134.*
7. *Moustafa, M.S., Pope, M.C., Mriheel, I.Y. (2019). High resolution sequence stratigraphy of the Middle–Late Triassic Al Aziziyah formation, northwest Libya. Journal of African Earth Sciences, 155, 75-89. DOI: https://doi.org/10.1016/j.jafrearsci.2019.03.009*
8. *Kamel, M., Tolba, A., AbuBakr, M.M., Omar, M.M. (2022). Utilization of Landsat-8 data for lithological mapping of neoproterozoic basement rocks in north Qena-Safaga road, North Eastern Desert, Egypt. Journal of African Earth Sciences, 186, 104420. DOI: https://doi.org/10.1016/j.jafrearsci.2021.104420*

9. *Marzouki, A., Dridri, A. (2023). Lithological discrimination and structural lineaments extraction using Landsat 8 and ASTER data: a case study of Tiwit (Anti-Atlas, Morocco). Environmental Earth Sciences, 82(125). DOI: https://doi.org/10.1007/s12665-023-10831-4*
10. *Ghrefat, H., Kahal, A.Y., Abdelrahman, K., Alfaifi, H.J., Qaysi, S. (2021). Utilization of multispectral landsat-8 remote sensing data for lithological mapping of southwestern Saudi Arabia. Journal of King Saud University - Science, 33(4), 101414. DOI: https://doi.org/10.1016/j.jksus.2021.101414*
11. *Santolaria, P., Ayala, C., Pueyo, E.L., Rubio, F.M., Soto, R., Calvin, P., Luzón, A., Rodríguez-Pintó, A., Oliván, C., Casas-Sainz, A.M. (2020). Structural and geophysical characterization of the western termination of the South Pyrenean triangle zone. Tectonics, 39(8). DOI: https://doi.org/10.1029/2019TC005891.*
12. *Saibi, H., Amir, G., Mohamed, F.S. (2019). Subsurface structural mapping using gravity data of Al-Ain Region, Abu Dhabi Emirate, United Arab Emirates. Geophysical Journal International, 216(2), 1201-1213. DOI: https://doi.org/10.1093/gji/ggy489*
13. *Yuan, Y., Gao, J.Y., Chen, L.N. (2016). Advantages of horizontal directional Theta method to detect the edges of full tensor gravity gradient data. Journal of Applied Geophysics, 130, 53-61. DOI: https://doi.org/10.1016/j.jappgeo.2016.04.009*
14. *Ibraheem, I.M., Haggag, M., Tezkan, B. (2019). Edge Detectors as Structural Imaging Tools Using Aeromagnetic Data: A Case Study of Sohag Area, Egypt. Geosciences 9(5), 211. DOI: https://doi.org/10.3390/geosciences9050211*
15. *IRC (Industrial Research Centre), 1985. Geological Map of Libya, 1:1,000,000. Industrial Research Centre, Libya.*
16. *El Hinnawy, M., Cheshitev, G. (1975). Geological map of Libya. Explanatory booklet, sheet Tarabulus NI 33-13. Industrial Research Centre, Tripoli.*
17. *Zaccagna, D. (1919). Itinerari geologici della Tripolitania occidental con appendic paleontologic. Mem. Descr. Carta Geol. Ital. XVIII, 126, Roma.*
18. *Lipparini, T. (1940). Tettonica e geomorfologia della Tripolitania. Bulletin of the Geological Society of Italy, Roma 59, 221-301.*
19. *Zivanovic, M. (1977). Geological map of Libya. Explanatory booklet, sheet Bani Walid NH 33-2. Industrial Research Centre, Tripoli.*
20. *Piccoli, G. (1971). Outlines of Volcanism in Northern Tripolitania. Symposium on the Geology of Libya, University of Libya, Tripoli 232–331.*
21. *Christie, A.M. (1966). Geology of Gharyan Area, Tripolitania, Libya. Ministry of Industry, Geological Section Bulletin, No. 5, Tripoli.*
22. *Liu, J.G., Phillippa, J.M. (2016). Image Processing and GIS for Remote Sensing: Techniques and Applications. Oxford: Wiley-Blackwell.*
23. *Lillesand, T.M., Kiefer, R.W. (2015). Remote Sensing and Image Interpretation. 7th Edition, Wiley, New York.*
24. *Abduh, A.G., Usman, F.C.A., Tampoy, W.M., Manyoe, I.N. (2021). Remote Sensing Analysis of Lineaments using Multidirectional Shaded Relief from Digital Elevation Model (DEM) in Olele Area, Gorontalo. Journal of Physics: Conference Series, 1783, 012095. DOI: https://doi.org/10.1088/1742-6596/1783/1/012095*
25. *Sabins, F.F., Ellis, J.M. (2020). Remote Sensing: Principles, Interpretation, and Applications, 4th ed.; Waveland Press: Long Grove, IL, USA.*
26. *Abdelsalam, M.G., Stern, R.J., Berhane, W.G. (2000). Mapping gossans in arid regions with Landsat TM and SIR-C images: the Beddaho alteration zone in northern Eritrea. Journal of African Earth Sciences, 30 (4), 903–916. DOI: https://doi.org/10.1016/S0899-5362(00)00059-2*
27. *S.P.L.A.J. (1979). Topographic map of Libya, 1:50,000. Polservice-Geokart, Poland.*
28. *Luirei, K., Lokho, K., Longkumer, L., Kothyari, G., Rai, R., Rawat, I.S., Nakhro, D. (2021). Morphotectonic evolution of the Quaternary landforms in the Yangui River basin in the Indo-Myanmar Range. Journal of Asian Earth Sciences, 218(15). DOI: https://doi.org/10.1016/j.jseaes.2021.104877*
29. *Wajid, A.A., Anees, M., Gorchani, J.K., Shahzad, K., Israr, A., Shafique, M. (2021). Lineament mapping for a part of the Central Sulaiman Fold–Thrust Belt (SFTB), Pakistan. Arabian Journal of Geosciences, 14, 1438. DOI: https://doi.org/10.1007/s12517-021-07784-y*
30. *Salawu, N.B, Olatunji, S., Adebiyi, L.S, Olasunkanmi, N.K, Dada, S.S. (2019). Edge detection and magnetic basement depth of Danko area, northwestern Nigeria, from low-latitude aeromagnetic anomaly data. SN Applied Sciences, 1, 1056. DOI: https://doi.org/10.1007/s42452-019-1090-3*

Authors Contribution: All authors have contributed equally to this work

Інтеграція дистанційного зондування та аеромагнітних даних для картографування літологічних і структурних ліній в Абу-Гайлан - Кікла - Тігрінна, північно-західна Лівія

Нуреддін Сааді [1],
доктор філософії (геологічна інженерія), викладач кафедри геологічної інженерії,
[1] Університет Тріполі, Університетська дорога, Тріполі, Лівія;
Усама Елкул [2],
магістр геології, викладач кафедри нафтової інженерії,
[2] Коледж інженерних технологій, Прибережна дорога, Джанзур, Лівія;
Салех А. Садег [1],
доктор філософії (геологічна інженерія),
професор кафедри інженерно-геологічних наук

У 1970-х роках Центр промислових досліджень у Лівії розпочав створювати геологічні карти всіх лівійських земель, отриманих з аналогових (друкованих) аерофотознімків і геологічних польових поїздок у деякі доступні місця. Останнім часом методи дистанційного зондування та інтеграції даних з використанням ГІС мають вирішальне значення для геологічної зйомки та картографування, що є корисним інструментом для вивчення та дослідження геології віддалених регіонів без необхідності фізичного доступу до них. Метою цього дослідження є картографування літологічних утворень і структурних ліній в регіоні Абу-Гайлан – Кікла – Тігрінна, північно-західна Лівія, використовуючи інтегровані дані дистанційного зондування та просторовий аналіз. Для картографування та аналізу літологічних і структурних ліній досліджуваної території були використані Enhanced Thematic Mapper Plus (ETM+), Satellite Pour l'Observation de la Terre (SPOT 5), European Remote-Sensing Satellite-2 (ERS-2), радар із синтетичною апертурою (SAR), C-діапазон, цифрова модель рельєфу (DEM), геологічні карти та аеромагнітні дані. Для розпізнавання літологічних одиниць протестовано різні злиті зображення та трансформації IHS. На основі спектральних характеристик і топографічних форм розпізнано та нанесено на карту літологічні та структурні лінеаменти. Витягнуті растри та векторні дані були інтегровані за допомогою методів дистанційного зондування та інтеграції даних ГІС. Мета наземної перевірки полягала в перевірці структурного відображення на основі ЦМР та ідентифікації будь-яких зсувів, потоків або долин, які можуть відображатися як краї в даних ЦМР. Крім того, визначено розташування штучних ліній, які з'являються на оброблених зображеннях у вигляді геологічних ліній і країв. Результати вказують на те, що дані дистанційного зондування були дуже корисними для розрізнення різних гірських порід і розпізнавання геологічних ліній у досліджуваній області. Створена літологічна карта показує п'ятнадцять геологічних утворень з очевидними і точними межами. Результати виявили нові геологічні лінементи на території дослідження. Напрямок вилучених геологічних ліній переважно північно-західний–південно-східний. Магнітні дані виявляють межі осадового басейну в районі дослідження. Глибина фундаменту в межах улоговини коливається від 122 метрів до 4,5 кілометрів. Витягнуті геологічні лінії були проаналізовані та інтерпретовані, щоб отримати більше інформації про основні структурні тенденції, що впливають на досліджувану територію. Методи, використані в цьому дослідженні для аналізу зображень дистанційного зондування та польових геологічних досліджень, можуть бути успішно використані в аналогічних регіонах Лівії.

Ключові слова*: Лівія, дистанційне зондування, цифровий рельєф, лінеаменти, літологічне картування, аеромагнітний, інтеграція даних.*

Внесок авторів: всі автори зробили рівний внесок у цю роботу

Надійшла 12 квітня 2023 р.
Прийнята 13 травня 2023 р.